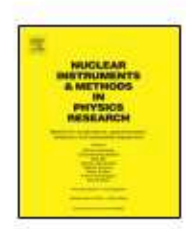
EI SEVIER

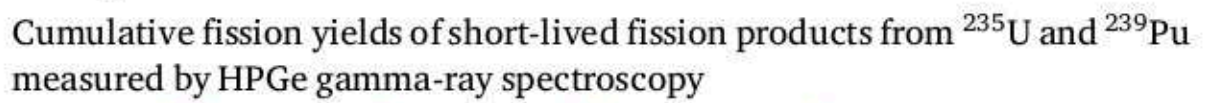
Contents lists available at ScienceDirect

# Nuclear Inst. and Methods in Physics Research, A

journal homepage: www.elsevier.com/locate/nima



# Full Length Article





- Brookhaven National Laboratory, PO Box 5000, Upton, NY, 11973, USA
- b Physics Department, Temple University, 1925 N. 12th St., Philadelphia, PA, 19122, USA
- 5 Oak Ridge National Laboratory, 1 Bethel Valley Rd., Oak Ridge, TN, 37830, USA

#### ARTICLE INFO

### Keywords: Cumulative fission yield Gamma-ray spectroscopy Nuckar data library

#### ABSTRACT

In this study, we present a preliminary investigation focused on determining cumulative fission yields for short-lived fission products. Our analysis involves examining gamma spectra from the irradiated samples of <sup>235</sup>U and <sup>239</sup>Pu using the High Flux Isotope Reactor. The motivation stems from the observed discrepancy in the antineutrino energy spectrum within the range of 5 to 7 MeV. While several hypotheses have been proposed, a thorough analysis of fission yields provides an additional way of gaining insight into this unexplained phenomenon. Our study suggests that the measured gamma rays from <sup>195</sup>Nb, <sup>140</sup>Cs and <sup>95</sup>Sr are consistent with the expected values. However, <sup>93</sup>Rb, <sup>96</sup>Y, <sup>97</sup>Y and <sup>142</sup>Cs cannot be quantified due to insufficient statistics, interference from other gamma rays and the Compton scattering background. Additionally, the calculated cumulative fission yields based on the measured <sup>140</sup>Cs and <sup>95</sup>Sr are found to be consistent with the JEFF3.3 fission yield library. The present work shows that the potential of improving gamma-ray spectroscopy in the fission yields as a means to improve our understanding of the antineutrino spectrum.

### 1. Introduction

Nuclear reactors are a large source of electron antineutrinos, making them indispensable for investigating the properties of these particles. Approximately 6 antineutrinos are generated from a single fission event, and therefore, a 1 GW thermal reactor emits about 10<sup>20</sup> antineutrinos per second [1,2]. In recent years, several reactor experiments were carried out to investigate various properties of the reactor antineutrino flavor oscillations (Daya Bay [3], RENO [4], STEREO [5], PROSPECT [6], NEOS [7], JUNO [8]) [2].

Experimental observations have revealed a spectral deviation in the 5 to 7 MeV range of antineutrinos when compared to the best available model. Currently, this spectral feature remains unexplained [9]. While Hayes et al. [10] have explored various potential sources contributing to this spectral deviation, Dwyer and Langford [11] have pointed out that several obvious systematic uncertainties such as absence of fission yields in the short-lived isotopes have not been considered in the summation method. They suggest that investigating fission yields could offer valuable insights into understanding this spectral deviation. Sonzogni et al. [12] re-evaluated the thermal and fast fission yields of 235U in the ENDF/B database. Their analysis revealed that the revision of thermal yields and decay probabilities for 86 Ge led to about 10%

variation in the calculated antineutrino spectrum in the 5 to 7 MeV energy range.

While measurement of fission yields from short-lived fission products remains challenging [13], this study represents a feasibility study for measurement of cumulative fission yields from short-lived fission products through gamma-ray measurements. In our analysis, measured cumulative fission yield is compared with the JEFF3.3 fission library to identify any disparities. The JEFF3.3 database is selected for the comparison because it is the preferred source of yields for antineutrino applications [9,14]. Selection of the short-lived fission products (Table 1) for our investigation is based on the list of significant contributors at 5.5 MeV in the antineutrino spectrum [11,12].

Unstable nuclides directly produced in fission undergo beta decay along the isobar chain. Although these beta decays have very short half-lives, they eventually yield nuclides with sufficiently long half-lives to allow measurement of emitted gamma rays [15]. The direct fission yield of individual nuclides in the primary fission event is referred to as Independent Fission Yield (IFY), while the total yield of a nuclide including beta decay feeding is termed Cumulative Fission Yield (CFY). These yields are expressed as per fission event [12,15].

<sup>\*</sup> Corresponding author at: Brookhaven National Laboratory, PO Box 5000, Upton, NY, 11973, USA. E-mail address: skim3@bnl.gov (S. Kim).

Present address: Thomas Jefferson National Accelerator Facility, 12000 Jefferson Av. Newport News, VA, 23606, USA.

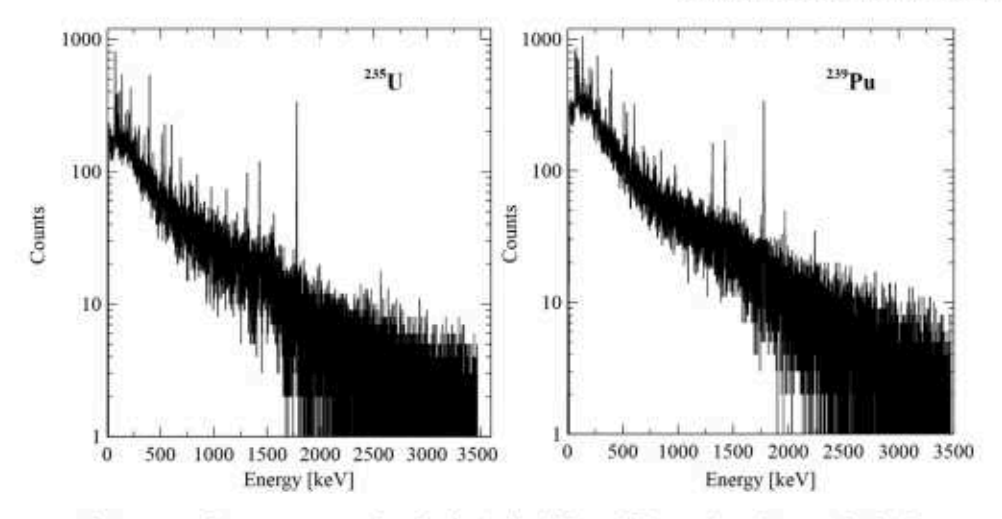


Fig. 1. Measured gamma-ray spectra from freshly irradiated 255U and 259Pu are plotted. See text for details.

Table 1
Decay data for 8 nuclides investigated in this study from the ENDF/B-VIII decay data sublibrary, including the decay chain gamma-ray with the strongest intensity selected for the present analysis. Uncertainty is given in the parenthesis.

Botope	Half life (s)	Gamma energy (keV)	Intensity	
<sup>93</sup> Rb	5.84(2)	432.61(3)	0.202(14)	
100Nb	1.4(2)	535.666(14)	0.46(6)	
<sup>141</sup> Cs	63.7(3)	602.25(5)	0.53(3)	
osSr .	23.90(14)	685.6	0.226	
<sup>02</sup> Rb	4.49(3)	814.98(3)	0.032(4)	
96Y	5.34(5)	1750.4(2)	0.0235(24)	
97Y	3.75(3)	3287.6(4)	0.181(19)	
140Cs	1.68(14)	359.598(14)	0.27(3)	

### 2. Experiment

The <sup>235</sup>U sample consists of 252.72 nanograms of natural uranium nitrate in an Inductively Coupled Plasma calibration solution. The <sup>239</sup>Pu sample consists of 301.3 nanogram of National Institute of Standards and Technology (NIST) Certified Reference Material (CRM-137). The samples are irradiated using the PT-2 pneumatic tube of the High Flux Isotope Reactor (HFIR) at the Neutron Activation Analysis laboratory (NAA) of Oak Ridge national Laboratory. The measured thermal and epithermal neutron fluxes at the irradiation location [16] are 4.59 × 10<sup>13</sup> n/cm<sup>2</sup>/s and 1.96E × 10<sup>11</sup> n/cm<sup>2</sup>/s respectively for <sup>235</sup>U, and 4.43 × 10<sup>13</sup> n/cm<sup>2</sup>/s and 3.24 × 10<sup>11</sup> n/cm<sup>2</sup>/s respectively for <sup>239</sup>Pu. The energy ranges for epithermal neutrons are 0.1 eV to 10 keV for <sup>239</sup>Pu and 1 eV to 10 keV for <sup>235</sup>U [17]. The neutron fluxes are measured using manganese and gold activation foils.

Each sample is irradiated for 30 s, and then transported to the detector chamber using the pneumatic tube transfer system [16] which introduces a 20-s delay prior to the gamma-ray measurement. Fig. 1 shows the measured gamma-ray spectra of the irradiated <sup>235</sup>U and <sup>239</sup>Pu. The gamma rays are measured with a 44% relative efficiency, ORTEC p-type coaxial HPGe detector with an aluminum end cap. Each sample is placed at 33 cm above the detector and measured for 30 s.

# 3. Fission yields and expected gamma rays

The expected gamma-ray yield calculation starts by determining the number of  $^{235}$ U and  $^{239}$ Pu nuclides initially present in the sample from the sample mass (m), Avogadro's number ( $N_A$ ) and the molar weight (M). The number of nuclides ( $N_{fd}$ ) directly produced from fission is given by Eq. (1).

$$N_{fd} = \text{IFY } \sigma_f \phi \frac{mN_A}{M} \tag{1}$$

The equation includes the IFY of a specific nuclide, the thermal neutron cross section  $(\sigma_f)$  and the thermal neutron flux  $(\phi)$  [18]. The IFY are tabulated in the JEFF3.3 library, and the neutron cross section is based on the ENDF/B-VIII.0 neutron cross section standard sublibrary. The JEFF3.3 and ENDF/B-VIII.0 fission yield libraries contain different IFY values for certain nuclides. This is demonstrated using the  $^{140}$ Cs decay chain in Table 2. In this example, JEFF3.3 does not have IFY for  $^{140}$ Sb, so the IFY value from ENDF/B-VIII.0 is used instead in our analysis. This suggests that  $N_{fd}$  will be different depending on the fission library used.

To determine the total number of nuclides  $(N_T)$  present at the end of irradiation,  $N_{fd}$  as well as each of its successors in the decay chain need to be determined from its own IFY and  $\beta$ -decayed. For the analysis presented in this work, only the  $\beta$ -decay path for the parent–daughter chains is used. The expected  $N_T$  is given in Eq. (2).

$$N_T = N_{fd} \frac{(1 - e^{-\lambda t})}{\lambda} + \sum_i Decay([N_{fd}]_j) \qquad (2)$$

The first term gives the total number of a gamma-ray emitting nuclide produced directly from IFY during the irradiation. The second term describes the total number of a gamma-ray emitting nuclide resulting from the  $\beta$ -decay of /th predecessor based on its own IFY.

In our study, the decay chains consist of 4 nuclides ( $^{93}$ Rb,  $^{142}$ Cs) and 6 nuclides ( $^{140}$ Cs,  $^{95}$ Sr,  $^{92}$ Rb,  $^{96}$ Y,  $^{100}$ Nb,  $^{97}$ Y). Each decay chain leading from IFY to the gamma-ray emitting nuclides measured in this study is described by a set of coupled linear differential equations describing the radioactive decays. These equations are reformulated as a set of matrices and solved using MATLAB [19]. The solution to each decay chain gives the number of a gamma-ray emitting nuclides produced from IFY and the decay of its predecessors during the 30-s irradiation. Fig. 2 summarizes the percent composition of the  $N_T$  based on the contribution from IFY and its successors. In general, only the parent or parent/grandparent of a given gamma-ray emitting nuclide remains at the end of irradiation. The nuclides further up in the decay chain have all decayed away due to their very short half-lives.

The uncertainty in the  $N_T$  is determined from the IFY of a gammaray emitting nuclide and its predecessors, their decay constants, and thermal neutron cross sections as shown in Eq. (3) [20]. The IFYs make a greater contribution to the overall uncertainty than  $\lambda$  and  $\sigma_f$ . For example, the IFYs accounts for 99% of the uncertainty in  $^{140}$ Cs and  $^{95}$ Sr for both  $^{235}$ U and  $^{239}$ Pu while the contributions from  $\lambda$  and  $\sigma$  are 1%.

$$\delta(N_T) = N_T \sqrt{\sum \left( \left( \frac{\delta(IFY)}{IFY} \right)^2 + \left( \frac{\delta(\lambda)}{\lambda} \right)^2 \right) + \left( \frac{\delta(\sigma_f)}{\sigma_f} \right)^2}$$
(3)

Finally, the expected gamma-ray yields  $(N_T)$  during the subsequent 30-s measurement time are calculated from the  $N_T$ , the decay constant

Table 2

Examples from the <sup>140</sup>Cs decay chain, showing the differing IFY of <sup>235</sup>U (top) and <sup>230</sup>Pu (bottom) from JEFF3.3 and ENDF/B-VIII.0 fission yield libraries. Uncertainty of each IFY is indicated in the parenthesis.

IFY	140 Sb	<sup>140</sup> Te	1401	140 Xe	140 Cs
JEFF3.3	No data	6.57E-08 (2.26E-08)	3.03E-04 (1.03E-04)	1.25E-02 (3.10E-03)	1.84E-02 (3.85E-03)
ENDF/B-VIII.0	2.82E-09 (1.81E-09)	9.04E-06 (5.78E-06)	1.11E-03 (7.13E-04)	2.59E-02 (1.04E-03)	3.05E-02 (1.83E-03)
IFY	(4) Sb	<sup>140</sup> Te	1401	140 Xe	<sup>141</sup> Cs
JEFF3.3	No data	2.33E-07 (8.06E-08)	4.77E-04 (1.63E-04)	1.83E-02 (4.06E-03)	2.18E-02 (4.52E-03)
ENDF/B-VIILO	5.61E-11 (3.59E-11)	1.41E-06 (9.02E-07)	5.94E-04 (3.80E-04)	1.54E-02 (4.31E-04)	2.28E-02 (3.64E-03)

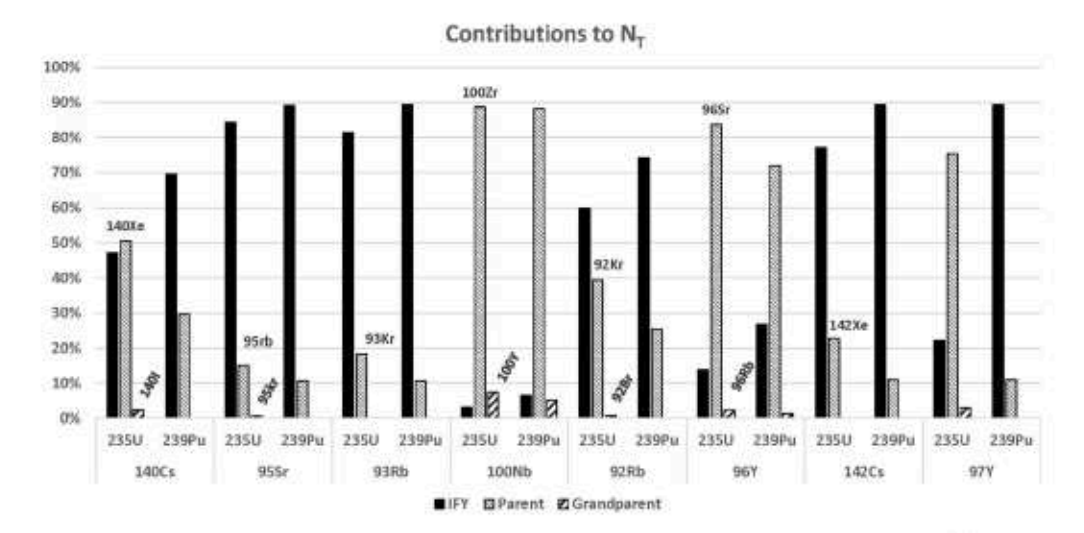


Fig. 2. The plot summarizes the percent contribution from the IFY and its successors to the composition of N<sub>T</sub> in our study. For example in <sup>208</sup>U, 47% of N<sub>T</sub> for <sup>140</sup>Cs is due to IFY of <sup>140</sup>Cs. The remaining contribution comes from <sup>140</sup>Se (51%, parent) and <sup>140</sup>Ic (2%, grandparent). The predecessors further up the decay chain such as <sup>140</sup>Se and <sup>140</sup>Te have all decayed away, and their contribution to <sup>140</sup>Cs is negligible. Nuclide labels for <sup>255</sup>U and <sup>259</sup>Pu are the same, and omitted in the <sup>259</sup>Pu portion of the chart for clarity.

( $\lambda$ ), the absolute efficiency ( $\epsilon$ ) of the HPGe, and the gamma emission intensity ( $I_{\tau}$ ). The calculation includes the contributions from the predecessors continuously decaying during the 20-s transportation delay. Except <sup>140</sup>Cs, the half-lives of the measured nuclides are much shorter than the detector measurement time, therefore, it is necessary to decay-correct the peak counts. The ANSI standard for the correction factor is described in Ref. [21]. The uncertainty in the expected gamma-ray yield,  $\delta(N_{\tau})$ , is evaluated through a quadrature sum of uncertainties in  $N_T$ ,  $\epsilon$ , and  $I_{\tau}$ . The dominant contributor to  $\delta(N_{\tau})$  comes from the  $\delta(N_T)$ . For example, 99% of the overall  $\delta(N_T)$  in <sup>140</sup>Cs and <sup>95</sup>Sr for both <sup>235</sup>U and <sup>239</sup>Pu can be attributed to  $\delta(N_T)$ .

# 4. Measured gamma rays

The energy and full width at half maximum (FWHM) calibrations of the HPGe detector have been determined by analyzing known gammaray peaks. The absolute efficiency of the detector is estimated using the Geometry and Tracking (GEANT4) [22] simulation package. In the simulation, 17 gamma-ray energies are selected to cover the energy range from 50 keV to 3.5 MeV. Each gamma-ray simulation was performed using 1E+6 photons to determine the efficiency of the detector at each photon energy. The detector model in GEANT4 includes all the details of detector construction, including a 0.1 cm thick aluminum window on the endcap of the detector and a 0.07 cm thick dead layer on the surface of the HPGe crystal. Dimensions of the HPGe were taken to be 6.5 cm in the diameter and 6.45 cm in the length based on published ORTEC documents [23]. According to the ANSI/IEEE standard 325 [24], the relative efficiency of an HPGe is defined by Eq. (4). The absolute efficiency of HPGe at 1.33 MeV is measured with a source to detector distance of 25 cm. The relative efficiency is the ratio of this HPGe absolute efficiency to the absolute efficiency of a 3-in, by 3-in, Na(Tl) scintillator at 1.33 MeV measured at 25 cm (1.2E-3).

Relative efficiency = 
$$\frac{\text{Absolute efficiency}}{1.2 \times 10^{-3}}$$
(4)

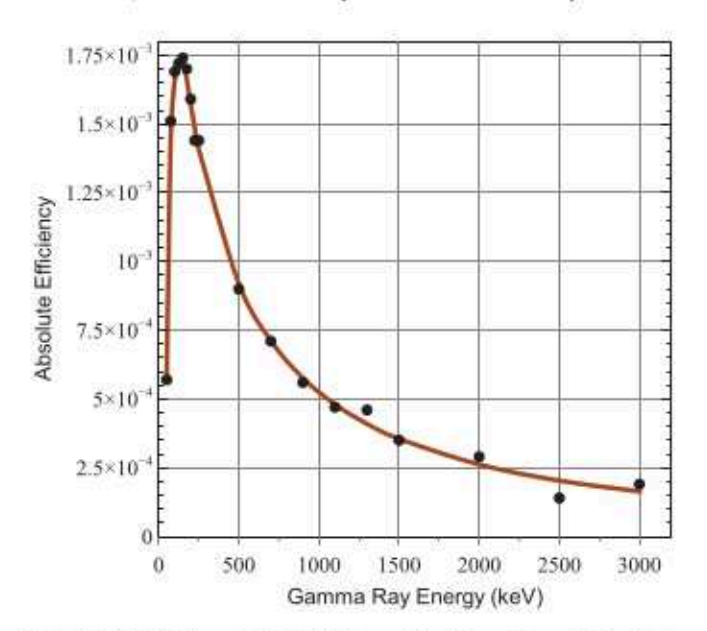


Fig. 3. GEANT4 efficiency for the ORTEC P-type 44% relative efficiency HPGe detector used here. The efficiency is fit using the parametric equation given in the RADWARE program.

To establish a benchmark, a GEANT4 simulation was performed for a point source placed at the standard distance of 25 cm from the detector. The absolute efficiency at 1333 keV was expected to be 5.3E-4 for a 44% relative efficient HPGe [25]. The simulated absolute efficiency was 5.9E-4(7.7E-5). Fig. 3 shows the simulated detector efficiency. The efficiency is fitted using the parametric equation given in the RADWARE software package [26]. Above 150 keV, efficiency is

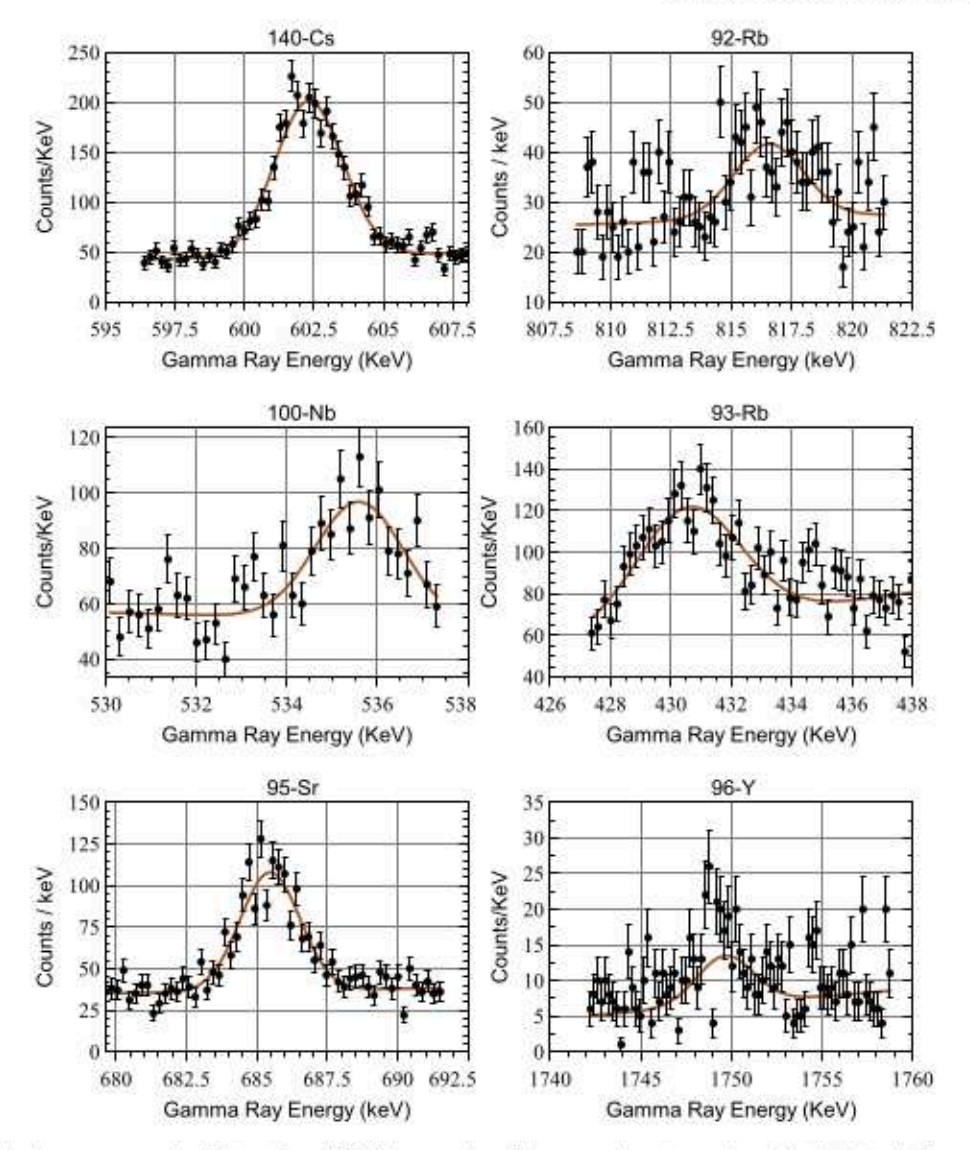


Fig. 4. Data and fits for the six gamma-ray peaks of interest from <sup>285</sup>U fission are shown. The measured spectra are shown by the dots with 1-σ uncertainties, and the fits by solid lines. Gamma ray peaks from <sup>97</sup>Y and <sup>142</sup>Cs are not detectable with the present statistics, and are omitted in this figure.

fitted with the parameters (D, E and F) in the form of:

$$Efficiency = e^{D+Ey+Fy^2}$$
(5)

where  $y = ln(E_y/1000)$  and  $E_y$  is a gamma-ray energy in keV.

Measured gamma-ray peaks are analyzed using two methods: nonlinear fitting and a simple summation. The ANSI standard for the summation method is given in [21,27,28], and the detailed explanation is given in [29,30]. Non-linear fit analysis is performed using a GF3M program from the RADWARE package [26] and an open-source software, GNUPLOT [31] (see Figs. 4 and 5).

The fitting algorithm offers a linear and a quadratic baseline fit. The linear baseline fit is chosen because it produces a less fitting error in the peak-count estimate than the quadratic fit. The linear baseline is given by A + Bx where A and B are fitted parameters, and x is a channel number. Initial estimate of A and B are given by a straight line between the limits of the fit. In the Gaussian profile, the fitted parameters are the position, height of the peak and the peak width (FWHM). The initial values for position and height are determined based on a given peak. To sufficiently account for the linear baseline as an approximation to the Compton continuum,  $3 \times FWHM$  from the centroid is chosen as a fitting range for a well isolated Gaussian peak [24,32].

Tables 3 and 4 summarize the fit results for <sup>235</sup>U and <sup>239</sup>Pu. In general, the fitted peak energies are consistent with tabulated values for

Table 3

Best-fit values and fitting statistics for the fission products from <sup>235</sup>U are summarized. Fitted energies are consistent with the calibrated energies. But fitted FWHMs show some divergence. The fit statistics (p-values) indicate acceptable fits for <sup>100</sup>Nb, <sup>140</sup>Cs and <sup>25</sup>Sr. (see Results section for detail).

235 U	χ <sup>2</sup> /DOF	Centroid		FWHM		p-value
		Calibrated	Fitted	Calibrated	Fitted	
HICs.	1.63	602.33	602.28(4)	1.93	2.87(8)	0.05
95 Sr	1.43	685.57	685.43(6)	2.01	2.50(11)	0.03
100 Nb	1.26	535.61	535.4(3)	1.87	2.4(10)	0.02
93 Rb	1.21	432.67	430.38(15)	1.76	3.4(3)	< 0.01
<sup>92</sup> Rb	2.26	814.98	814.6(5)	2.12	1.1(12)	< 0.01
96 Y	1.62	1750.50	1749.4(3)	2.73	1.9(6)	< 0.01

both <sup>235</sup>U and <sup>239</sup>Pu. However, the p-values and FWHM fits suggest that a single Gaussian may be a poor model for some peaks, likely indicating interference from additional unidentified gamma rays. This could be clarified with improved counting statistics. As shown in Fig. 1, <sup>239</sup>Pu generates generally more gamma-ray activities than <sup>235</sup>U, suggesting more interference. This fact appears to be consistent with all p-values being lower for <sup>239</sup>Pu compared to <sup>235</sup>U.

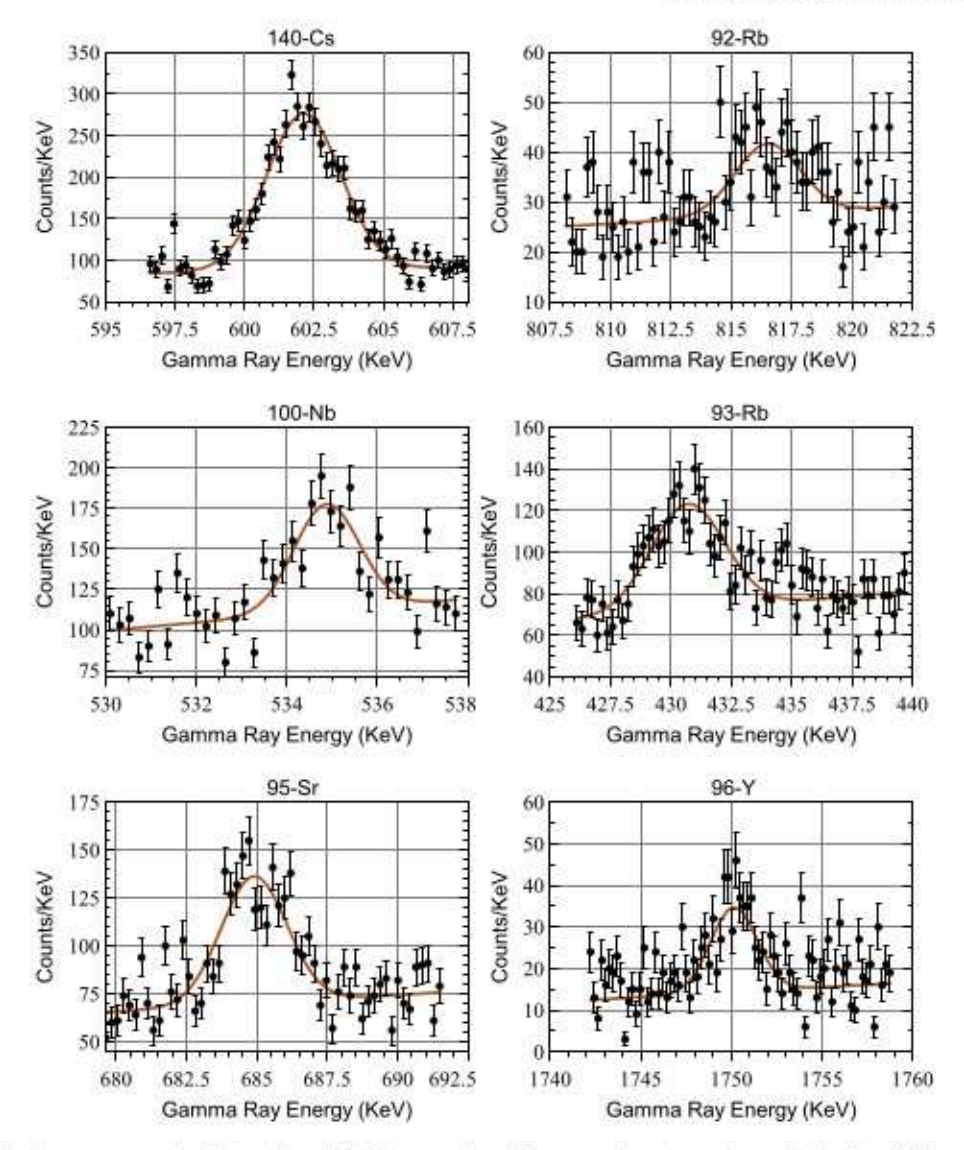


Fig. 5. Data and fits for the six gamma-ray peaks of interest from <sup>29</sup>Pu fission are shown. The measured spectra are shown by the dots with 1-σ uncertainties, and the fits by solid lines. Gamma ray peaks from <sup>17</sup>Y and <sup>1-2</sup>Cs are not detectable with the present statistics, and are omitted in this figure.

Table 4

Best-fit values and fitting statistics for the fission products from <sup>299</sup>Pu are summarized. Similar to the case of <sup>288</sup>U, fitted energies are consistent with the calibrated energies while fitted FWHMs show some divergence. Unlike <sup>285</sup>U, the fit statistics (p-values) indicate poor fit quality for <sup>100</sup>Nb, <sup>140</sup>Cs and <sup>95</sup>Sr due to interference from other gamma rays. (see Results section for detail).

255U	$\chi^2/\text{DOF}$	Centroid		FWHM		p-value
		Calibrated	Fitted	Calibrated	Fitted	
140Cs	1.90	602.33	602.03(5)	1.93	3.41(11)	< 0.01
<sup>95</sup> Sr	1.37	685.57	685.45(6)	2.01	2.41(11)	< 0.01
moNb	2.74	535.61	534.75(10)	1.87	2.09(23)	< 0.01
93Rb	2.92	432.68	434(10)	1.76	5(18)	< 0.01
92Rh	1.89	814.96	815.4(3)	2.12	1.9(10)	< 0.01
96Y	1.9	1750.50	1750.19(13)	2.73	2.23(23)	< 0.01

### 5. Cumulative fission yields from measured gamma rays

The cumulative fission yield is calculated by evaluating the disintegration rate of nuclides relative to the total fission rate, and is given in Eq. (6) [33]. The disintegration rate of nuclides at the end of irradiation is derived from the measured gamma-ray counts, including appropriate adjustments for delay and count corrections. The overall fission rate is determined by the number of <sup>235</sup>U (<sup>239</sup>Pu) in the sample, the thermal fission cross-section, and the thermal neutron flux.

$$CFY = \frac{\lambda N_p}{N_{fd} I_{\gamma} \epsilon (1 - e^{-\lambda t_{fr}})(e^{-\lambda t_d})(1 - e^{-\lambda t_w})}$$
(6)

In Eq. (6),  $N_p$  is the measured gamma-ray peak count based on  $N_T$ ,  $t_{tr}$  is the irradiation time (30 s),  $t_d$  is the transport delay time (20 s) and  $t_m$  is the detector count time (30 s). Because the gamma-ray peak counts for  $^{93}{\rm R}$  b,  $^{92}{\rm R}$  b and  $^{96}{\rm Y}$  are below the statistical limit of detection, proper  $N_p$  cannot be determined. The fission-produced  $^{100}{\rm Nb}$  at the end of irradiation has almost all decayed away during the 20-s transport delay due to its short half life (1.5 s), and is not detectable by the HPGe during the measurement time. The measured 100Nb gamma rays are primarily due to the decay of  $^{100}{\rm Zr}$  (7.1 s).  $N_p$  from  $^{140}{\rm Cs}$  and  $^{95}{\rm Sr}$  are appropriate to use for calculating CFY. The uncertainty in the calculated CFY,  $\delta(CFY)$ , is determined through a quadrature using  $N_p$ ,  $\lambda$ ,  $\epsilon$  and  $I_r$ .

# 6. Results

For each gamma-ray, the statistical significance is determined using the method of Refs. [27,29,30]. This method involves two statistical limits: Lc and Ld. The critical limit (Lc) is defined as the net count of a gamma ray peak above which a sample net count is statistically significant with the probability of false positive given by  $\alpha$ . The detection limit (Ld) is defined as the net count of a gamma ray peak above Lc that has a probability of false negative given by  $\beta$ . We adopt the usual convention of using  $\alpha = \beta = 0.05$  as the desired level of statistical significance. We note that the statistics in this method are based on a one-sided 95% confidence level so that the z statistic cutoff is 1.65, not 1.96. For the non-linear fitting method, Lc and Ld are given by Eqs. (7) and (8) where  $\sigma = \sqrt{B}$  and B = background count (no sample is present) respectively [29].

$$L_c = 2.33 \sigma$$
 (7)

$$L_d = 2.71 + 4.65 \sigma$$
 (8)

In Figs. 6 and 7, the measured gamma rays for <sup>100</sup>Nb, <sup>140</sup>Cs and <sup>95</sup>Sr are statistically significant, are above the minimum detection limit, and are fully consistent with the expected counts.

For <sup>93</sup>Rb, <sup>92</sup>Rb, and <sup>96</sup>Y, the obtained net counts from fitting significantly exceed the expected values. Using multiple Gaussian peaks does not improve the fitting results for <sup>93</sup>Rb and <sup>92</sup>Rb. In the case of <sup>96</sup>Y (1750.4 KeV), separation of <sup>96m</sup>Y (1750.06 KeV) from <sup>96</sup>Y cannot be achieved in the current data. Therefore, we estimate the gamma ray interference as follows.

For  $^{93}$ Rb, 6 nuclides (A = 90, 134, 138, 143, 144, 145) produce a similar or larger order of magnitude of gamma-ray yield ( $I_{\gamma} \times$  total fission yield) in the 432 keV region in our data [34,35]. Based on the estimate of the gamma rays having a measurable effect, the proportion of gamma-ray yield of  $^{93}$ Rb with respect to the 6 nuclides gives about 6% which is consistent with the expected net count of  $^{93}$ Rb. In addition,  $^{143}$ Ba (431.2 KeV,  $I_{\gamma} = 0.0276$ ) is expected to produce approximately the same number of gamma ray counts in our data as  $^{93}$ Rb (432.61 KeV,  $I_{\gamma} = 0.202$ ), and is shown to be consistent with  $^{93}$ Rb.

As for <sup>92</sup>Rb, 13 nuclides (A = 82, 91, 92, 101, 132, 133, 132, 136, 137, 139, 140, 144, 147) produce a similar or larger order of magnitude of gamma-ray yields than <sup>92</sup>Rb in the 815 keV energy region [34,35]. The proportion of measured peak counts from <sup>92</sup>Rb with respect to the thirteen nuclides is about 1.4% which is consistent with the expected net count of <sup>92</sup>Rb. For <sup>239</sup>Pu, 1% of the contribution in the 815 keV region is due to <sup>92</sup>Rb alone.

96mY has a larger gamma-ray intensity (0.88) than 96Y(0.024), and larger IFY from 235U(0.011) and 239Pu(0.014) compared to 96Y: 235U(0.006) and 239Pu(0.008). The fission analysis shows that 3% (1%) of the gamma ray yield is due to 96Y alone for 235U(239Pu). When fitted net counts are adjusted appropriately to account for interference, they are shown to be consistent with the expected net count. However, the results are below the statistical significance and are inconclusive.

Due to their statistical insignificance of gamma-ray peak counts, the computations of CFY for  $^{93}$ Rb,  $^{92}$ Rb, and  $^{96}$ Y have been excluded. Similarly, the calculation of CFY for  $^{100}$ Nb is excluded because it is undetectable by the HPGe detector during the measurement. CFY values for  $^{140}$ Cs and  $^{95}$ Sr have been calculated and are shown in Fig. 8 ( $^{235}$ U) and Fig. 9 ( $^{239}$ Pu) alongside the JEFF3.3 fission yield data for comparison. The primary sources of uncertainty in  $\delta(CFY)$  come from the uncertainties associated with  $N_p$  and  $\epsilon$ . This indicates that enhancing the statistics for gamma-ray peak counts and refining efficiency calibration can result in a better estimation of CFY.

Hayes et al. [1] draw attention to the possibility of a contribution from epithermal neutron-induced fission. In this study, the highest neutron flux is observed at 0.02 eV within the thermal neutron range. Consequently, the recorded epithermal neutron flux accounts for just 0.4% (0.7%) of the thermal neutron flux for <sup>235</sup>U (<sup>239</sup>Pu). This implies that the number of neutrons interacting with <sup>235</sup>U (<sup>239</sup>Pu) in the thermal region is 234(137) times greater than in the epithermal region. In our analysis, the contribution from epithermal neutrons is deemed too minimal to significantly impact the fission yield data.

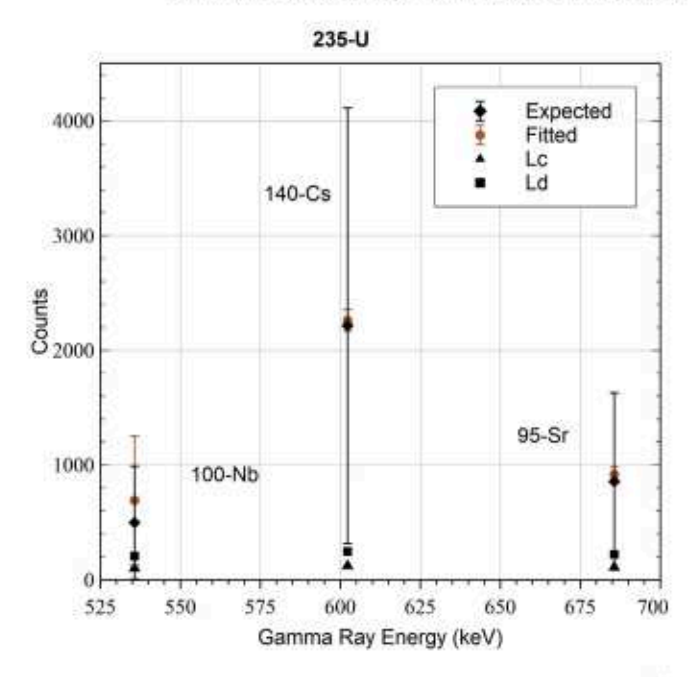


Fig. 6. Fitted and expected net counts and statistical limits and uncertainties for <sup>288</sup>U. The yields of <sup>100</sup>Nb, <sup>148</sup>Cs and <sup>95</sup>Sr are shown to be consistent with the expected values. <sup>95</sup>Rb, <sup>92</sup>Rb and <sup>96</sup>Y are below the statistical limit of detection, and are excluded from the plot for clarity.

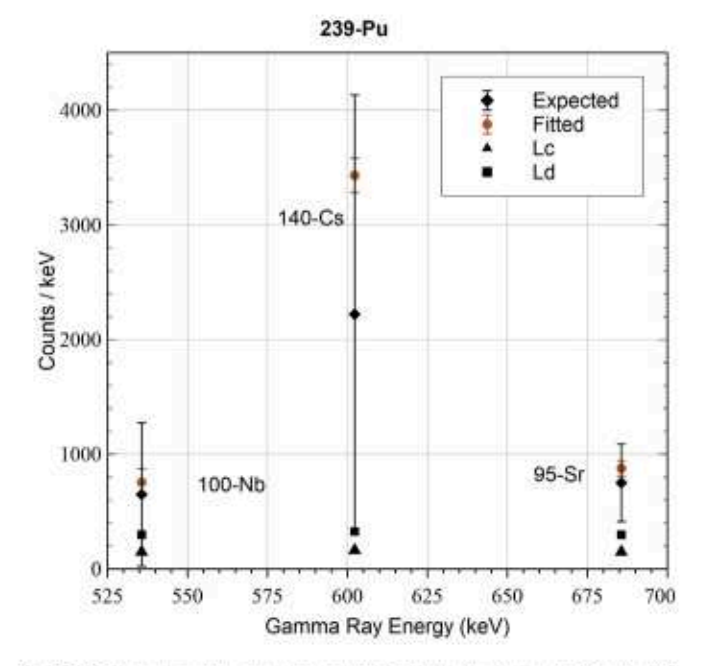


Fig. 7. Fitted and expected net counts and statistical limits and uncertainties for <sup>239</sup>Pu. The yields of <sup>100</sup>Nb and <sup>95</sup>Sr are plotted and shown to be consistent with the expected values. The fitted <sup>141</sup>Cs is about 35% larger than the expected value, suggesting a possible problem with the JEFF3.3 fission yield library. <sup>95</sup>Rb, <sup>92</sup>Rb and <sup>96</sup>Y are below the statistical limit of detection, and are excluded from the plot for clarity.

### 7. Conclusion

Certain nuclides make substantial contributions to the antineutrino spectrum in the 5 to 7 MeV range. An examination of their fission yields provides valuable insights for comprehending the unexplained spectral deviation in this energy range. In this study, we determine the cumulative fission yields of specific short-lived fission products from the irradiated <sup>235</sup>U and <sup>239</sup>Pu using the gamma-ray spectroscopy.

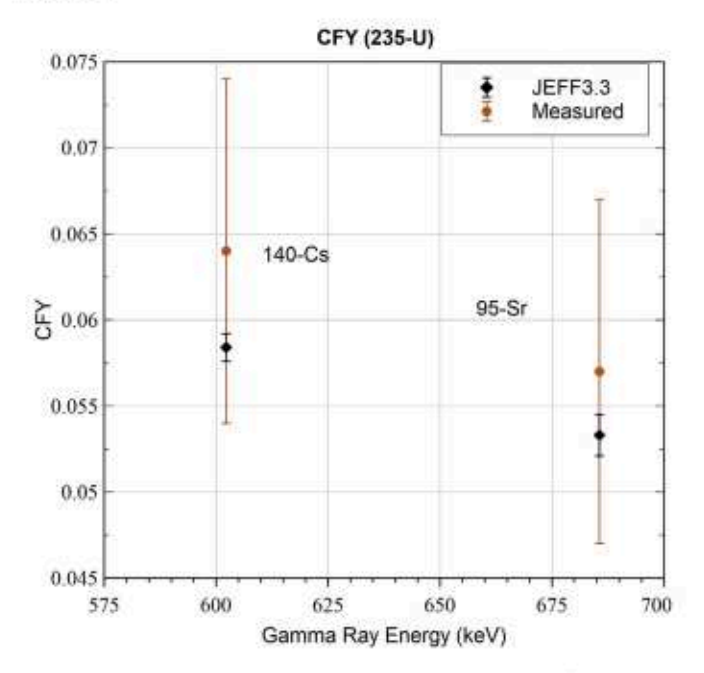


Fig. 8. Comparison of measured CFY and JEFF3.3 library CFY from <sup>28</sup>U. Within the uncertainty, measured CFY are consistent with JEFF3.3 CFY.

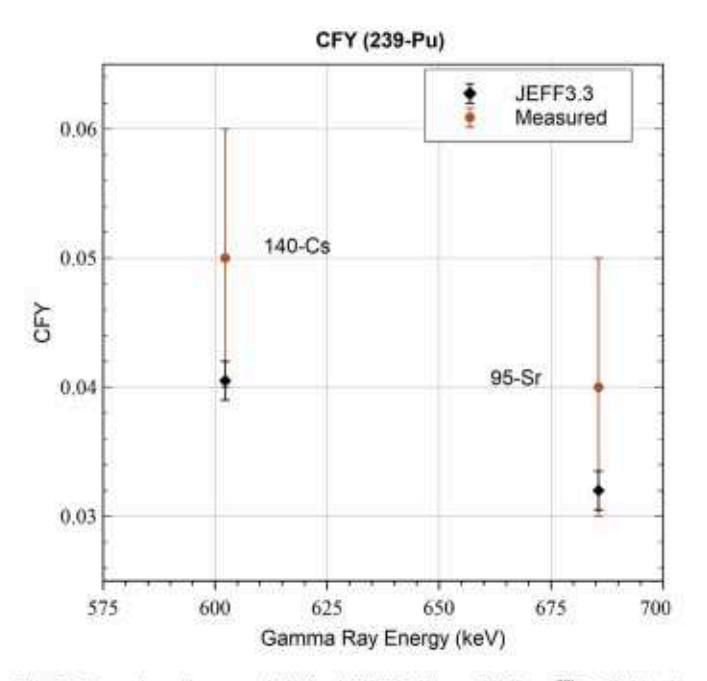


Fig. 9. Comparison of measured CFY and JEFF3.3 library CFY from <sup>299</sup>Pu. Within the uncertainty, measured CFY are consistent with JEFF3.3 CFY except <sup>566</sup>Y. Measured CFY for <sup>566</sup>Y is about 5 factors larger than CFY from JEFF3.3.

The measured gamma rays for <sup>100</sup>Nb, <sup>140</sup>Cs and <sup>95</sup>Sr are consistent with the expected. Statistics for the measured <sup>91</sup>Rb, <sup>92</sup>Rb and <sup>96</sup>Y are sub-optimal due to interference from other gamma rays and Compton background. The gamma ray peaks from <sup>97</sup>Y and <sup>142</sup>Cs are undetectable due to low fission yield, limited detector efficiency, and environmental background. Because of its short half-life, we are unable to calculate the CFY for <sup>100</sup>Nb. The calculated CFY for <sup>140</sup>Cs and <sup>95</sup>Sr are in agreement in comparison with the JEFF3.3 database.

A follow-up experiment offers the opportunity to improve various aspects of the current preliminary study. The primary source of uncertainty comes from IFY measurements, which need separate and dedicated experiments to refine their accuracy. To prevent the loss of nuclides, it is essential to reduce the 20-s transport delay. For instance, all fissioned 100Nb nuclides decay during the transport delay due to its short 1.5-s half-life. Addressing this challenge may require a substantial reconstruction of the sample transportation apparatus, incurring significant expenses. Additional improvements include the integration of multiple HPGe detectors to enhance gamma-ray detection through coincidence measurements, as well as installing better shielding to minimize background interference. The fission analysis could be improved by incorporating additional decay paths, such as beta-delayed-neutron emissions and isomers. But this would significantly increase the complexity of the analysis, necessitating the use of more advanced software tools. Although CFY measurements show consistency, a subsequent study can further enhance their accuracy by accounting for correction factors such as beam fluctuations and gamma-ray attenuation.

### Declaration of competing interest

The authors declare that they have no known competing financial interests or personal relationships that could have appeared to influence the work reported in this paper.

#### Data availability

The authors do not have permission to share data.

### Acknowledgments

Authors would like to thank A. Sonzongni and E. McCutchan for valuable comments. This work was funded by the U.S. National Science Foundation under grant NSF-PHY1242611, NSF-1812504, 1747523, and 1314483. The work at Brookhaven National Laboratory was sponsored by the Office of Nuclear Physics, Office of Science of the U.S. Department of Energy under Contract No. DE-AC02-98CH10886 with Brookhaven Science Associates, LLC.

### References

- A.C. Hayes, P. Vogel, Reactor neutrino spectra, Annu. Rev. Nucl. Part. Sci. 66 (2016) 219-244.
- [2] L.A. Bernstein, D.A. Brown, A.J. Koning, B.T. Rearden, C.E. Romano, A.A. Sonzogni, A.S. Voyles, W. Younes, Our future nuclear data needs, Annu. Rev. Nucl. Part. Sci. 69 (2019) 109–136.
- [3] F. An, W. Bai, A. Balantekin, M. Bishai, S. Blyth, G. Cao, J. Cao, J. Chang, Y. Chang, H. Chen, et al., Improved measurement of the evolution of the reactor antineutrino flux and spectrum at daya bay, Phys. Rev. Lett. 130 (21) (2023) 211801.
- [4] S. Yoon, H. Seo, Z. Atif, J. Choi, H. Jang, J. Jang, S. Jeon, K. Joo, K. Ju, D. Jung, et al., Measurement of reactor antineutrino flux and spectrum at RENO, Phys. Rev. D 104 (11) (2021) L111301.
- [5] STEREO neutrino spectrum of 235U fission rejects sterile neutrino hypothesis, Nature 613 (7943) (2023) 257-261.
- [6] M. Andriamirado, A. Balantekin, C. Bass, D. Bergeron, E. Bernard, N. Bowden, C. Bryan, R. Carr, T. Classen, A. Conant, et al., Final measurement of the U 235 antineutrino energy spectrum with the PROSPECT-I detector at HFIR, Phys. Rev. Lett. 131 (2) (2023) 021802.
- [7] Y. Ko, B. Kim, J. Kim, B. Han, C. Jang, E.J. Jeon, K. Joo, H. Kim, H. Kim, Y. Kim, et al., Sterile neutrino search at the NEOS experiment, Phys. Rev. Lett. 118 (12) (2017) 121802.
- [8] JUNO physics and detector, Prog. Part. Nucl. Phys. 123 (2022) 103927, http://dx.doi.org/10.1016/j.ppnp.2021.103927.
- [9] P. Dimitriou, B. Littlejohn, M. Fallot, Nuclear Data for Antineutrino Spectra and their Applications, Tech. rep., NA, 2019.
- [10] A. Hayes, J. Friar, G. Garvey, D. Ibeling, G. Jungman, T. Kawano, R.W. Mills, Possible origins and implications of the shoulder in reactor neutrino spectra, Phys. Rev. D 92 (3) (2015) 033015.
- [11] D. Dwyer, T. Langford, Spectral structure of electron antineutrinos from nuclear reactors, Phys. Rev. Lett. 114 (1) (2015) 012502.
- [12] A. Sonzogni, E. McCutchan, T. Johnson, P. Dimitriou, Effects of fission yield data in the calculation of antineutrino spectra for U-235 (n, fission) at thermal and fast neutron energies, Phys. Rev. Lett. 116 (13) (2016) 132502.
- [13] S. Leoni, C. Michelagnoli, J. Wilson, Gamma-ray spectroscopy of fission fragments with state-of-the-art techniques, La Rivista Nuovo Cimento 45 (7) (2022) 461–547.

- [14] H.P. Mumm, C. Romano, N. Bowden, A. Conant, R. Goldblum, P. Huber, J. Link, B. Littlejohn, J.P. Ochoa-Ricoux, S. Prasad, et al., Nuclear data to reduce uncertainties in reactor antineutrino measurements, 2022.
- [15] I. Ahmad, W. Phillips, Gamma rays from fission fragments, Rep. Progr. Phys. 58 (11) (1995) 1415.
- [16] ORNL, High Flux Isotope Reactor (HFIR) User Guide A guide to in-vessel irradiations and experiments, URL https://www.neutrons.orul.gov/sites/default/ files.
- [17] B. Littlejohn, A. Conant, D. Dwyer, A. Erickson, I. Gustafson, K. Hermanek, Impact of fission neutron energies on reactor antineutrino spectra, Phys. Rev. D 97 (7) (2018) 073007.
- [18] J. Knowles, S. Skutnik, D. Glasgow, R. Kapsimalis, A generalized method for characterization of <sup>235</sup>U and <sup>239</sup>Pu content using short-lived fission product gamma spectroscopy, Nucl. Instrum. Methods Phys. Res. A 833 (2016) 38–44.
- [19] T.M. Inc., MATLAB version: 9.13.0 (r2022b), 2022, URL https://www.mathworks.com.
- [20] J. Taylor, An Introduction To Error Analysis: The Study of Uncertainties in Physical Measurements, second ed., University Science Books, California, 1997.
- [21] American national standard for calibration and use of germanium spectrometers for the measurement of Gamma-ray emission rates of radionuclides, 1999, ANSI N42.14-1999.
- [22] S. Agostinelli, J. Allison, K.a. Amako, J. Apostolakis, H. Araujo, P. Arce, M. Asai, D. Axen, S. Banerjee, G. Barrand, et al., GEANT4—a simulation toolkit, Nucl. Instrum. Methods Phys. Res. A 506 (3) (2003) 250–303.
- [23] E.G. Roth, HPGe detectors at ORTEC/AMETEK 12, Ortec, 2018, [link]. https://wasabi.physics.unc.edu/event/10/contributions/78/attachments/51/52/ ORTEC-PIRE-GEMADARC Knoxville Dec 2018.pdf.

- [24] E. Fairstein, S. Wagner, et al., IEEE standard test procedures for germanium gamma-ray detectors, IEEE std 325-1996, 1996.
- [25] ORTEC, Overview of Semiconductor Photon Detectors, Ortec. [link]. https://www.ortec-online.com/~/media/ametekortec/other/overview-of-semiconductor-photon-detectors.
- [26] D. Radford, RadWare Software Package (2011).
- [27] Multi-Agency Radiological Laboratory Analytical Protocols Manual, EPA 402-B-17-001 III (20), 2004.
- [28] High Resolution Gamma-Ray Spectrometry Analyses For Normal Operations and Radiological Incident Response, EPA 402-B-17-001, 2019.
- [29] G.F. Knoll, Radiation Detection and Measurement, John Wiley & Sona, New York, 2000.
- [30] G. Gilmore, Practical Gamma-Ray Spectroscopy, John Wiley & Sons, New York, 2008.
- [31] T. Williams, C. Kelley, R. Lang, D. Kotz, J. Campbell, Gruplot, 2004.
- [32] L. Costrell, M. Unterweger, N. Ahmad, American national standard for calibration and use of germanium spectrometers for the measurement of gamma-ray emission rates of radionuclides, The Institute of Electrical and Electronics Engineers Inc. NY, 1999.
- [33] M.E. Gooden, C. Arnold, J. Becker, C. Bhatia, M. Bhike, E. Bond, T. Bredeweg, B. Fallin, M. Fowler, C. Howell, et al., Energy dependence of fission product yields from 235U, 238U and 239Pu for incident neutron energies between 0.5 and 14.8 MeV, Nucl. Data Sheets 131 (2016) 319–356.
- [34] J.W. Robinson, M.P. Dion, G.C. Eiden, O.T. Farmer, M. Liezers, RadiCalc: a program for estimating radiation intensity of radionuclide mixtures, J. Radionnal, Nucl. Chem. 303 (2015) 1955–1960.
- [35] A. Croff, ORIGEN2: a revised and updated version of the oak ridge isotope generation and depletion code, 1980.